

# The impact of ionic strength on the adsorption of protons, Pb, Cd, and Sr onto the surfaces of Gram negative bacteria: testing non-electrostatic, diffuse, and triple-layer models

D.M. Borrok\*, J.B. Fein

*Department of Civil Engineering and Geological Sciences, University of Notre Dame, 156 Fitzpatrick Hall, Notre Dame, IN 46556, USA*

Received 21 October 2004; accepted 11 January 2005

Available online 11 February 2005

## Abstract

Bacterial surface adsorption reactions are influenced by electric field effects caused by changes in ionic strength; however, existing datasets are too sparse to definitively constrain these differences or to determine the best way to account for them using thermodynamic models. In this study, we examine the ionic strength dependence of proton and metal adsorption onto the surfaces of *Pseudomonas mendocina* and *Pseudomonas putida* by conducting proton, Cd(II), Pb(II), and Sr(II) adsorption experiments over the ionic strength range of 0.001 to 0.6 M. Chosen experimental results are thermodynamically modeled using a non-electrostatic approach, a diffuse layer model (DLM), and a triple-layer model (TLM). The results demonstrate that bacterial surface electric field effects are negligible for proton, Cd, and Pb adsorption onto *P. putida* and *P. mendocina*, and that the discrete site non-electrostatic model developed in this study is adequate for describing these reactions. The extent of Sr adsorption is influenced by changes in the bacterial surface electric field; however, the non-electrostatic model better describes Sr adsorption behavior than the DLM or TLM. The DLM and TLM greatly overpredict the effect of the electric field for all adsorption reactions at all ionic strengths tested.

© 2005 Elsevier Inc. All rights reserved.

**Keywords:** Bacteria; Adsorption; Diffuse layer; Triple layer; Electrostatic; Cd; Sr; Pb

## 1. Introduction

Negatively charged organic-acid functional groups present on bacterial cell walls can adsorb significant concentrations of aqueous metal cations [1,2]. Because bacteria are abundant in most near-surface geologic settings [3], they may be important in controlling the availability and cycling of trace metals [4,5], and in the fate and transport of heavy metal contaminants [6]. Because of their environmental significance, a range of thermodynamic models have been developed to describe bacterial surface adsorption reactions (e.g., [7–11]). Several studies have suggested that electric double-layer interactions on the bacterial surface play an important role in proton and metal binding [7,10,12,13], and a

number of different surface electric field models have been adopted to account for these effects. For example, numerous studies have adopted a constant capacitance electrostatic approach, relating surface charge to surface potential using an arbitrarily assigned capacitance value [8,14–16]. Other workers [7,10,17] have adopted the Donnan electrostatic model, which invokes the assumption that all counter ions necessary to balance the bacterial surface charge are homogeneously distributed within the hydrated bacterial cell wall volume [18]. This Donnan volume can either be empirically derived, estimated, or directly measured using transmission electron microscopy.

However, despite the seemingly large number of proposed thermodynamic models and electrostatic treatments, very few studies have examined the effect of ionic strength on bacterial adsorption reactions over a broad range of electrolyte concentration (>1 order of magnitude, e.g., [10]).

\* Corresponding author.

E-mail address: [dborrok@nd.edu](mailto:dborrok@nd.edu) (D.M. Borrok).

Moreover, a number of studies have arbitrarily assigned electrostatic correction factors for data collected at a single ionic strength (e.g., [8,15]). Other studies have focused on bacterial cell wall components which, although useful, may not be entirely representative of the bacterial surface electric field in systems with whole cells [7,12]. Finally, there is little agreement among studies as to the magnitude of ionic strength effects on bacterial surface adsorption reactions or as to whether these effects are unique for each bacterial species of interest.

Ledin et al. [19] measured the extent of metal (Cs, Sr, Eu, Zn, Cd, Hg) adsorption onto the Gram negative bacterium *Pseudomonas putida*, and found that the extent of adsorption for all of these metals decreased with increasing ionic strength (0.01 to 0.1 M). However, the magnitude of this increase was relatively insignificant for Cs, Eu, and Hg. Daughney and Fein [13] examined the ionic strength dependence of proton and metal (Cd, Cu, Pb) binding onto two Gram positive bacteria (*B. subtilis* and *B. licheniformis*) by performing acid–base titrations and metal adsorption experiments at ionic strengths of 0.01 and 0.1 M. The proton binding constants used to fit the titration data in this study were roughly similar for each ionic strength; however, apparent site densities for both bacteria increased slightly in response to increased salt concentration. The metal binding results from this study were difficult to interpret in that the extent of metal binding onto *B. subtilis* generally decreased with increasing ionic strength, while the extent of metal binding onto *B. licheniformis* generally increased with increasing ionic strength. Cox et al. [9] also measured proton binding to *B. subtilis* over the more narrow ionic strength range of 0.025 to 0.1 M, and similarly described a resultant increase in apparent site density with increasing salt concentration. Hass and Dichristina [20] observed almost no effect on the adsorption of protons and U(VI) to the surface of the Gram negative bacterium, *Shewanella putrefaciens*, over the ionic strength range of 0.02 to 0.1 M. Small et al. [21] demonstrated that the concentration of Sr adsorbed to the surface of *Shewanella alga* decreased as ionic strength increased from a very low value (dilute) to 0.1 M. Martinez et al. [10] performed acid–base titrations of *B. subtilis* and the Gram negative bacterium *Escherichia coli* at ionic strengths of 0.01, 0.05, 0.1, and 0.5 M. They describe a decrease in apparent total site density with increasing ionic strength for *B. subtilis*. Conversely, the apparent total site density for *E. coli* increased when ionic strength was raised from 0.01 to 0.05 M, but remained constant at higher ionic strengths. Yee et al. [17] observed large decreases in the extents of adsorption of Sr, Ba, and Ca to the surface of *B. subtilis* as ionic strength increased from 0.001 to 0.1 M. These studies suggest that the relationship between ionic strength and bacterial surface adsorption reactions is highly dependent upon the component adsorbed (i.e., different behaviors exist for protons and various metals), but that the magnitude of electrostatic effects may not be dependent upon which bacterial species is involved. However, existing datasets are simply

too sparse to definitively constrain these differences or to determine the best way to account for them using thermodynamic models.

In this study, we expand our understanding of the ionic strength dependence of proton and metal adsorption onto bacterial surfaces by conducting proton, Cd, and Pb adsorption experiments at ionic strengths of 0.01, 0.1, and 0.5 M, using *Pseudomonas mendocina* and *Pseudomonas putida*. These species were chosen for study because they are common Gram negative aerobes found in near-surface geologic systems, and very few studies have examined the effect of ionic strength on metal adsorption onto Gram negative bacterial surfaces. We supplement traditional pH-edge adsorption experiments with Cd, Pb, and Sr ionic strength isotherm experiments (constant pH experiments with variable ionic strength, 0.001 to  $\sim$ 0.6 M). We use a discrete site surface complexation modeling approach to determine best-fit stability constants and site densities for selected datasets. Modeling parameters are constrained using a non-electrostatic approach to quantify and examine the magnitude of the effect of ionic strength on proton and metal binding reactions. The non-electrostatic modeling results are then compared to model parameters developed using diffuse layer and triple-layer electrostatic treatments.

## 2. Materials and methods

### 2.1. Bacteria and growth conditions

*P. mendocina* is a strictly aerobic, Gram negative, rod-shaped bacterium approximately 2  $\mu$ m long and 0.5 to 1  $\mu$ m wide, and was isolated from near-surface soils at the Nevada test site [22]. *P. putida* is an aerobic Gram negative bacterium of similar dimensions that was purchased from American Type Culture Collection (#33015).

Bacteria were initially cultured in 3 ml of trypticase soy broth with 0.5% yeast extract for 24 h at 32 °C, then transferred to 1 L of broth of the same composition and grown for another 24 h at 32 °C. Bacteria were harvested from the growth media by centrifugation, transferred to test tubes, and washed five times in a NaClO<sub>4</sub> electrolyte solution. The ionic strength of the wash solution was chosen to match that of the experiment in which the bacteria were to be used. NaClO<sub>4</sub> was chosen as the experimental electrolyte because the perchlorate anion does not form complexes to an appreciable extent with protons, Cd<sup>2+</sup>, Pb<sup>2+</sup>, or Sr<sup>2+</sup>, under the experimental conditions. During each wash, the bacteria were suspended in fresh electrolyte solution using a vortex machine and stir rod. Bacteria were centrifuged for 5 min at 8000 rpm ( $\approx$ 7150g) to form a pellet at the base of the test tube and the electrolyte was discarded. After the final wash, the bacteria were placed in weighed test tubes and centrifuged (7000 rpm ( $\approx$ 5500g) at 25 °C) for 1 h, stopping three times to decant all supernatant. After 1 h, the mass of the moist bacterial pellet was determined. The mass

recorded during this step is the wet mass we report throughout this study. This wet mass is approximately 5 times more than the dry mass of the bacteria [11]. The bacterial pellet was immediately used in potentiometric titrations or in Cd adsorption experiments. Although the bacterial cells remain visually intact after this treatment (when observed using an environmental scanning electron microscope (ESEM) [23]), they are not expected to be metabolizing during experiments because of the lack of electron donors and nutrients and because of the short (<3 h) experimentation times.

## 2.2. Potentiometric titration experiments

Titration experiments were performed (in triplicate) on suspensions of *P. mendocina* and *P. putida*. Bacteria were harvested from the growth media and washed as described above. They were then suspended in approximately 10 ml of 0.01, 0.1, or 0.5 M NaClO<sub>4</sub> that had been purged of CO<sub>2</sub> by N<sub>2</sub> bubbling for 60 min. The suspension was immediately placed into a sealed titration vessel maintained under a positive pressure of N<sub>2</sub>. Titrations were conducted using an automated burette assembly. Each suspension was first titrated to the desired starting pH of ~2.5, using minute aliquots of 1.040 N HNO<sub>3</sub>. Base titrations were then performed using aliquots of 1.028 N NaOH. Titrations were performed to a maximum pH of 9.7 to avoid cellular damage to the bacteria. During each titration, the suspension reached a stability of 0.001 pH units/s prior to the addition of the next aliquot of acid or base. The total volume of acid and base added during each of the titrations ranged from about 3.0 to 3.5% of the starting volume of the solution.

## 2.3. Cd and Pb adsorption and kinetics experiments

Cd adsorption experiments were conducted at 0.1 M ionic strength in batch reaction vessels using 10 and 3 g/L *P. mendocina* and *P. putida*. Pb adsorption experiments were conducted in the same fashion using 3 and 0.5 g/L *P. mendocina* and 3 and 1 g/L *P. putida*. Additional experiments at ionic strengths of 0.01 and 0.5 M were conducted for the 10 g/L Cd and the 0.5 and 1 g/L Pb experiments for each bacteria type. Because Cd and Pb have very different binding affinities for the bacterial surface, it was necessary to adjust the bacteria:metal ratio for these experiments accordingly to ensure adsorption edges would occur over the tested pH range. All experiments were conducted using 10 ppm (10<sup>-4.05</sup> M Cd and 10<sup>-4.32</sup> M Pb) of the chosen metal (diluted from a 1000 ppm atomic absorption standard). The upper pH of the Pb adsorption experiments was purposefully limited to values of about pH 6.5, because aqueous Pb-hydroxide and Pb-carbonate species become increasingly important above this pH. We cannot accurately constrain binding constants for these additional Pb species without additional experiments conducted over a broad range of pH and carbonate concentrations.

The pH of the metal stock solution was adjusted to circumneutral values prior to the addition of bacteria to avoid acid shock to the cells. The weighed bacterial pellets were suspended in the metal-bearing electrolyte (NaClO<sub>4</sub>) stock solution and gently stirred until homogeneously distributed. Approximately 10 ml aliquots of the homogeneous bacteria–metal–electrolyte suspensions were transferred into individual batch reaction vessels. The pH of each batch experiment was adjusted to the desired value using small volumes of 0.01 or 0.1 M NaOH or HNO<sub>3</sub>. Each batch experiment was then allowed to equilibrate on a rotating rack for 2 h (*P. mendocina*) or 4 h (*P. putida*), and the equilibrium pH was measured (equilibration times were determined through kinetics experiments described below). Each sample was then centrifuged, filtered through a 0.45 μm nylon syringe filter membrane, acidified to prevent precipitation, and analyzed for the dissolved metal using an inductively coupled plasma–atomic emission spectroscopy (ICP–AES) technique. Calibration standards were made using the same electrolyte used in the experiments. Analytical uncertainty for most samples was determined to be less than approximately ±2%. Samples from the 0.5 M electrolyte experiments were diluted 5 times and internally spiked with a Y standard prior to analyses using the ICP–AES technique described above. Analytical uncertainty for these samples was greater, ranging from ±2 to 5%. The accuracy of several of the 0.5 M Cd samples was further tested using an element two-sector field ICP–mass spectrometer (MS). Uncertainties for the ICP–MS samples were about ±1%, and proved to be similar (within error) of the ICP–AES results. The decrease in aqueous metal concentration that occurred during each experiment was attributed to metal adsorption onto the bacterial cell wall. Control experiments in our laboratory (data not shown) have demonstrated that metal adsorption onto the experimental apparatus is negligible.

Adsorption and desorption kinetics experiments were conducted using 10 g/L *P. mendocina* and *P. putida*. These experiments were conducted to define an adequate equilibration time for the metal adsorption experiments and to verify the reversibility of the adsorption reactions. Washed bacteria were suspended in stock solutions of 10 ppm Cd and 0.1 M NaClO<sub>4</sub> and gently agitated using a stir bar. During the adsorption kinetics experiments, the starting pH of each stock solution (2.8) was rapidly raised to (and held at) ≈4.0 using small aliquots of 1.0 or 0.1 M NaOH. 10 ml aliquots of the bacteria–metal–electrolyte suspension were removed as a function of time, centrifuged, filtered, acidified, and later analyzed for dissolved Cd using the ICP–AES technique described above. The metal–electrolyte–bacteria stock solutions for the desorption experiments were gently agitated with a stir bar and allowed to equilibrate for 4 h at pH ~ 7.5 (it was determined that about 90% of total Cd was adsorbed at this pH). The pH of the desorption stock solutions were then lowered to ~4.0 using aliquots of 1.0 or 0.1 M HNO<sub>3</sub>. 10 ml aliquots of the bacteria–metal–electrolyte suspension were removed as a function of time.

The vessels were promptly centrifuged, filtered, acidified, and analyzed for Cd as described previously.

#### 2.4. Ionic strength isotherm experiments with Sr, Cd, and Pb

Ionic strength isotherm experiments for Sr, Cd, and Pb were conducted using 10 ppm of each metal and 6, 3, and 1 g/L of *P. putida*, and 6, 3, and 0.5 g/L of *P. mendocina*. Bacteria were initially suspended in a pH-neutral stock solution of 0.001 M NaClO<sub>4</sub> with the chosen metal, and the suspension was continuously mixed using a magnetic stir bar and plate. During the initial portion of the experiment, the pH of each stock solution was held constant at a pH ~ 6.0 through the addition of small aliquots of 0.01 or 0.1 M NaOH or HNO<sub>3</sub>. The pH was held at this value because earlier adsorption experiments indicated that a significant portion of the total metals would be adsorbed under these conditions. After 2 h of equilibration time at pH ~ 6.0, 10 ml aliquots of the homogeneous bacteria–metal–electrolyte suspensions were transferred into individual batch reaction vessels. The ionic strength of each reaction vessel was adjusted to the desired value through the addition of small concentrations of reagent grade, crystalline NaClO<sub>4</sub>. Using this technique, the error associated with calculating ionic strength for each reaction vessel is estimated to be about ±5%. Each batch experiment was then allowed to equilibrate on a rotating rack for 2 h (*P. mendocina*) or 4 h (*P. putida*), and the equilibrium pH was measured. The vessels were then centrifuged, filtered, acidified, and analyzed for the experimental metal using the ICP–AES technique described previously. However, in this case numerous calibration standards and dilutions were necessary in order to closely match the electrolyte concentration of the standards to that of each batch experiment. Analytical uncertainty for these samples was about ±3%.

### 3. Modeling approach

#### 3.1. Discrete site surface complexation model

We use a discrete site surface complexation approach to model titration and metal adsorption data. This approach has been described previously [8,11,23,24], and a brief overview is presented below. We represent the deprotonation of organic-acid functional groups on the bacterial surface with a number of discrete monoprotic acids according to the reaction

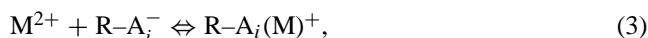


where R is the bacterium to which the functional group type A<sub>i</sub> is attached. The proton binding constant, K<sub>a</sub>, for reaction (1) can be expressed as

$$K_a = \frac{[\text{R-A}_i^-]a_{\text{H}^+}}{[\text{R-A}_i\text{H}^0]}, \quad (2)$$

where [R–A<sub>i</sub><sup>–</sup>] and [R–A<sub>i</sub>H<sup>0</sup>] represent the concentration of deprotonated and protonated sites, respectively, for site A<sub>i</sub>, and a<sub>H<sup>+</sup></sub> represents the activity of protons in the bulk solution. The number of discrete surface binding site types, the concentration of each site, and the proton binding stability constant for each site are determined through the modeling of the potentiometric titration data.

We represent metal adsorption onto the bacterial surface as an interaction between an aqueous metal cation (M<sup>2+</sup>) and a deprotonated surface site to form a bacterial surface complex according to the reaction



with a stability constant, K, for this reaction given by

$$K = \frac{[\text{R-A}_i(\text{M})^+]}{a_{\text{M}^{2+}}[\text{R-A}_i^-]}, \quad (4)$$

where [R–A<sub>i</sub>(M)<sup>+</sup>] is the concentration of the bacterial surface complex of interest, and a<sub>M<sup>2+</sup></sub> is the aqueous activity of the metal cation.

Our model is a simplification of what is likely an extremely complex chemical system, and should not be treated as an exact representation of the chemical speciation and mechanisms involved. We assume a 1:1 (metal:ligand) complexation stoichiometry for all adsorption reactions in our study. However, if actual complexation stoichiometries vary from the assumed reactions, predictions of metal complexation under conditions where bacterial surface sites become saturated (e.g., higher metal:bacteria ratios than tested in our study) could be erroneous. Moreover, if additional complexation mechanisms not tested in our study become significant under extremely low or extremely high metal:bacteria ratios, equilibrium constants for these reactions must be included to predict complexation with bacterial surfaces under these conditions.

#### 3.2. Model calculations

We utilize the program FITEQL 2.0 to solve for functional group site concentrations and proton and metal binding stability constants [25]. The relative goodness of fit of each tested model is quantified using the residual function, V(Y), from the FITEQL 2.0 output for each model. Lower V(Y) values signify better fits, and V(Y) values between 0 and 20 can generally be considered good fits [25].

Activity coefficient corrections are made within FITEQL using the Davies equation. Application of the Davies equation to systems with ionic strengths greater than about 0.1 M can introduce errors in calculated activity coefficients. However, activity coefficients for ions in our study calculated using the Davies equation are within 0.03 to 0.04 units of the activity coefficients for these ions calculated using the extended Debye–Hückel equation, which has been calibrated for high ionic strengths [26]. Because activities are not assigned for bacterial surface species and the activity of protons in solution (pH) is a measured quantity that is input

into FITEQL as serial data, very small errors are associated with the application of the Davies equation for models in our study. These errors are well within acceptable limits because they allow us to achieve a consistent comparison among different models at different ionic strengths that would not otherwise be possible. Aqueous metal hydroxide species in each experimental system are accounted for in our models using equilibrium constants from Baes and Mesmer [27].

### 3.3. Bacterial surface electric field models

The problem of how to best account for electric field effects on bacterial surface adsorption reactions is not straightforward. The characteristics of the bacterial surface are in many ways more like those of organic macromolecules (e.g., humic and fulvic acids) than those of mineral surfaces. For example, the functional groups present on mineral surfaces can be assumed to occupy the outer surface of a rigid plane, while those on bacterial surfaces are present throughout a semi-rigid, three-dimensional fabric of substantial thickness. Organic macromolecules are similar to bacterial surfaces in that functional groups associated with the molecules occupy a three-dimensional polyelectrolytic mixture of aliphatic and aromatic hydrocarbons, but are different in that their structure is much less rigid than that of a bacterial cell wall or a mineral surface. Functional groups present on the surfaces of specific oxide minerals are often assumed to be of the same character and to possess identical binding affinities (i.e., a single site modeling approach can be used to describe them). Conversely, bacterial surfaces contain a number of chemically distinct functional groups that can only be mechanistically described using multi-site models. Chemical [28,29] and spectroscopic [30–33] evidence suggests that carboxyl, phosphoryl, hydroxyl, and amine moieties can be important proton-active functional groups on most bacterial surfaces. Similarly, chemically distinct carboxyl and phenolic functional groups are present in humic and fulvic acids. Finally, mineral surfaces typically have a definable zero point of charge (ZPC) because the functional groups present on their surfaces become doubly protonated and positively charged at low pH. This ZPC concept is not directly applicable to bacterial surfaces. The monoprotic, organic-acid functional groups present on the bacterial surface do not become doubly protonated and positively charged at low pH. Although electrophoretic mobility studies suggest that some bacterial species can carry a net positive charge at very low pH (largely below 3.0; e.g., [17]), this does not mean that the critical organic-acid functional groups become doubly protonated or that one can use this information to define a true ZPC for bacterial species. Organic macromolecules are similar to bacterial surfaces in that they are absent of a true ZPC, carrying a net negative charge over the pH range for which they are dissolved (largely over 2.0). Hence, the approaches used to describe electric field interactions for mineral surfaces (e.g., double-layer and triple-layer models) may not be

directly applicable for describing electric field interactions with bacterial surfaces.

In our study, we use a non-electrostatic modeling approach to quantifying the effect of ionic strength on modeling parameters. This is an appropriate first step, because only after we have defined the type and magnitude of electrostatic effects on bacterial surface adsorption reactions can we determine what kind of electrostatic corrections must be made to account for them. Hence, the parameters we develop using the non-electrostatic approach are ‘apparent’ parameters because they can change in response to changes in the electric field surrounding the bacterial surface. Alternately, intrinsic modeling parameters are referenced to the condition of zero surface charge and are unaffected by changes in ionic strength. The relationship between an apparent stability constant and an intrinsic stability constant can be expressed according to the following reaction,

$$K_{\text{apparent}} = K_{\text{intrinsic}} \exp(-\Delta Z F \Psi / RT), \quad (5)$$

where  $F$  and  $R$  are Faraday’s constant and the ideal gas constant, respectively,  $T$  is absolute temperature,  $\Delta Z$  is the change in the charge of the surface species in the reaction, and  $\Psi$  is the electric field potential [34]. The value for  $\Psi$  is calculated using one of the various surface electric field models that relate surface charge to electric potential. Application of a surface electric field model requires knowledge of the specific surface area of the solid. The uncertainties involved in cell density and cell geometry calculations are large. Hence, we assign the value previously calculated by Fein et al. [8] for *B. subtilis* (140 m<sup>2</sup>/wet gram) for the surfaces of *P. mendocina* and *P. putida*.

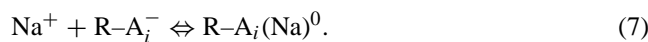
We also use the diffuse layer model (DLM) within FITEQL to solve for proton binding stability constants and functional group site concentrations for comparison to the non-electrostatic modeling results. This approach uses the Gouy–Chapman–Stern–Grahame relationship to relate surface potential ( $\Psi$ ) to surface charge ( $\sigma$ ) according to the following equation,

$$\Psi = (2RT/zF) \sinh^{-1} \left( \frac{\sigma}{\sqrt{8RT \varepsilon \varepsilon_0 c}} \right), \quad (6)$$

where  $z$  and  $c$  are the valence and concentration of the counterion, respectively,  $\varepsilon$  is the dielectric constant of water, and  $\varepsilon_0$  is the vacuum permittivity [34]. The diffuse layer treatment is advantageous in that there are no empirically derived parameters associated with its application; however, this same fact renders the approach rather inflexible.

We also use the triple-layer model (TLM) approach in some examples for comparison to the non-electrostatic and DLM approaches. The triple-layer approach is the most common surface electric field model for mineral surfaces. It is based on the idea that charge is developed at the surface of the mineral ( $O$ -plane) and electrolyte counterions in solution form complexes with the mineral surface functional group sites beginning some distance away from the surface ( $\beta$ -plane). The diffuse layer is present some distance away

from the counterion complexes, beginning at the  $d$ -plane. Each plane of charge has its own electric potential and the system can be modeled as a set of parallel plate capacitors. Hence, adjustable parameters for the TLM include  $C_1$  (the capacitance between the first two planes) and  $C_2$  (the capacitance between the next two planes) [35]. Although they can be measured or predicted in theory, the stability constant values for electrolyte complexation with surface functional groups ( $K_{\text{cation}}$  and  $K_{\text{anion}}$ ) are also treated as adjustable parameters in practice [36,37]. Because of the differences between bacterial surfaces and mineral surfaces, we must modify the TLM somewhat for our application. For example, because we use a discrete number of monoprotic acids to represent bacterial surface functional group sites, the sites never become positively charged. Hence, we cannot define a stability constant for the electrolyte anion in solution binding to a positively charged functional group site ( $K_{\text{anion}}$ ). We define the stability constant,  $K_{\text{cation}}$  (the electrolyte cation,  $\text{Na}^+$ , binding to a negatively charged functional group site), according to the following reaction:



Also, the TLM is most often used with a single-site modeling approach; however, we adapt it for use in a multi-site system.

## 4. Experimental and modeling results

### 4.1. Potentiometric titration experiments

*P. putida* and *P. mendocina* exhibit significant buffering capacity over the entire pH range studied (about 2.5 to 9.7), and the titration curves are similar in shape and position to each other as well as to those determined previously for a number of individual bacterial species (e.g., [8,14]) and consortia of bacterial species [11,38]. The shapes and positions of the titration curves for each bacterial species change slightly as a function of ionic strength from 0.01 to 0.5 M. The titration data (reported as  $\text{H}^+$  consumed per wet gram of bacteria) for *P. putida* and *P. mendocina* are presented in Figs. 1 and 2, respectively.

We first model the titration data using the non-electrostatic approach to determine apparent proton binding constants ( $K_a$  values from Eq. (2)) and apparent site densities for each bacterium at each ionic strength. We determine the minimum number of discrete functional group sites that are required to account for the buffering capacity of each bacterial suspension by sequentially testing models with one through five proton-active sites. Models with four proton binding sites yield significantly better fits to each of the titration datasets at each of the ionic strengths than models with fewer sites. In each case, five site models do not converge, indicating that they are underconstrained and that the data do not support a non-electrostatic model with five or more

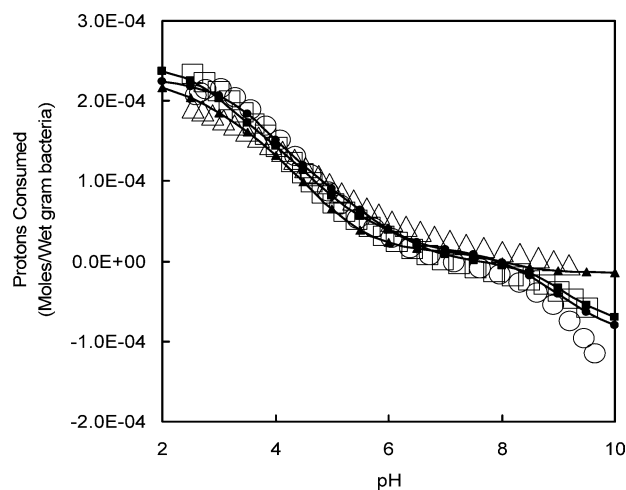


Fig. 1. Potentiometric titration data for *P. putida* reported as  $\text{H}^+$  consumed per gram of bacteria with average best-fit curves for the non-electrostatic model (solid curve and squares), DLM (solid curve and triangles), and TLM (solid curve and circles). Data for only one of the three titrations performed at each ionic strength are shown for clarity. Values are positive for net acid consumed; negative for net base consumed. ( $\Delta$ ) 0.01 M ionic strength data, ( $\square$ ) 0.1 M ionic strength data, and ( $\circ$ ) 0.5 M ionic strength data.

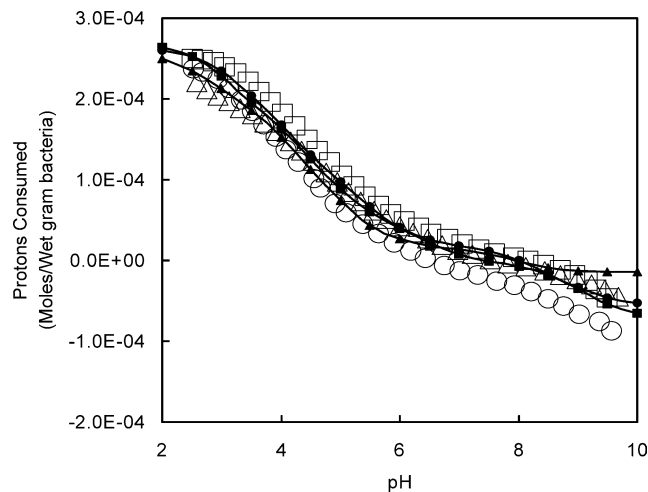


Fig. 2. Potentiometric titration data for *P. mendocina* reported as  $\text{H}^+$  consumed per gram of bacteria with average best-fit curves for the non-electrostatic model (solid curve and squares), DLM (solid curve and triangles), and TLM (solid curve and circles). Data for only one of the three titrations performed at each ionic strength are shown for clarity. Values are positive for net acid consumed; negative for net base consumed. ( $\Delta$ ) 0.01 M ionic strength data, ( $\square$ ) 0.1 M ionic strength data, and ( $\circ$ ) 0.5 M ionic strength data.

discrete sites. The averaged apparent proton binding constants, apparent site densities, and  $V(Y)$  values for the best-fit *P. putida* and *P. mendocina* models at each ionic strength are compiled in Tables 1 and 2, respectively. The average non-electrostatic model fits for all the ionic strength data for each bacterium are presented with the original data in Figs. 1 and 2, respectively. We define the four discrete functional group sites with the lowest to highest  $\text{p}K_a$  ( $-\log K_a$ ) values for *P. putida* as sites 1 through 4, respectively, and those for *P. mendocina* as sites A through D, respectively.

Table 1

Average non-electrostatic, DLM, and TLM proton binding stability constants and functional group site concentrations for triplicate *P. putida* titrations performed at three different ionic strengths

Ionic strength	V(Y)	Proton binding stability constants (pK <sub>a</sub> )				Functional group site concentrations (mol/wet gram)				
		1	2	3	4	1	2	3	4	Total <sup>a</sup>
<i>Four-discrete-site non-electrostatic model</i>										
0.01 M										
Average	0.94	2.84	4.68	6.33	9.16	8.71E-5	9.09E-5	4.83E-5	4.40E-5	2.7E-4
Std. dev.	0.33	0.37	0.13	0.14	0.11	4.28E-5	9.15E-6	6.88E-6	3.93E-6	4.5E-5
0.1 M										
Average	0.59	3.04	4.57	6.34	9.18	9.30E-5	1.17E-4	5.28E-5	6.21E-5	3.3E-4
Std. dev.	0.07	0.06	0.02	0.02	0.02	5.09E-6	3.53E-6	1.32E-6	1.95E-6	6.6E-6
0.5 M										
Average	1.34	3.67	4.96	6.52	9.20	1.13E-4	8.85E-5	4.21E-5	1.32E-4	3.8E-4
Std. dev.	0.87	0.18	0.23	0.19	0.08	1.63E-5	1.90E-5	8.57E-6	1.01E-5	2.8E-5
<i>Two-site diffuse layer electrostatic model</i>										
0.01 M										
Average	8.29	2.24	4.94	NA	NA	1.83E-4	4.71E-5	NA	NA	2.3E-4
Std. dev.	0.72	0.13	0.39	NA	NA	1.72E-5	5.56E-6	NA	NA	1.8E-5
0.1 M										
Average	5.74	2.76	5.74	NA	NA	2.39E-4	5.97E-5	NA	NA	3.0E-4
Std. dev.	0.35	0.05	0.12	NA	NA	3.96E-6	7.19E-7	NA	NA	4.0E-6
0.5 M										
Average	6.77	3.65	7.55	NA	NA	2.33E-4	1.49E-4	NA	NA	3.8E-4
Std. dev.	1.47	0.03	0.23	NA	NA	7.68E-6	3.39E-5	NA	NA	3.5E-5
<i>Three-site triple-layer electrostatic model</i>										
0.01 M										
Average	5.78	1.94	3.14	5.76	NA	8.28E-5	9.95E-5	4.27E-5	NA	2.3E-4
Std. dev.	4.84	0.39	0.35	0.56	NA	6.64E-6	1.56E-5	8.58E-6	NA	1.8E-5
0.1 M										
Average	2.08	3.02	4.16	7.07	NA	1.36E-4	9.35E-5	6.29E-5	NA	2.9E-4
Std. dev.	0.62	0.24	0.46	0.36	NA	2.26E-5	1.98E-5	4.41E-6	NA	3.0E-5
0.5 M										
Average	1.36	4.05	5.16	8.44	NA	1.56E-4	8.26E-5	2.11E-4	NA	4.5E-4
Std. dev.	0.41	0.05	0.06	0.10	NA	8.02E-6	4.03E-6	4.54E-5	NA	4.6E-5

FITEQL was used to calculate pK<sub>a</sub> values based on Eq. (2) in the text,  $K_a = [R-A_i^-]a_{H^+}/[R-A_iH^0]$ . NA, not applicable for model.

<sup>a</sup> Total functional group site concentrations.

Modeling results indicate that the pK<sub>a</sub> values for each bacterium are very similar (Tables 1 and 2). Fig. 3 presents the pK<sub>a</sub> values for each bacterial species as a function of ionic strength. Although the pK<sub>a</sub> values for site 1 (lowest *P. putida* pK<sub>a</sub>) increase slightly with increasing ionic strength, the other pK<sub>a</sub> values for both bacterial species exhibit little or no dependence upon salt concentration (Fig. 3). The apparent total site densities (the sum of the concentrations of binding sites for each of the four discrete sites) for *P. putida* and *P. mendocina* are within 2σ uncertainties of each other, as compared at each ionic strength (Fig. 4). However, the apparent total site densities for both bacteria increase with increasing ionic strength. The apparent site density for *P. putida* increases by about 40% over the ionic strength range of 0.01 to 0.5 M, while the apparent site density for *P. mendocina* increases by about 20% over the same range (Fig. 4).

The titration data were remodeled using the DLM approach for comparison to the non-electrostatic approach. We again determine the minimum number of discrete functional

group sites required to account for the buffering capacity of each bacterial suspension by sequentially testing models with one through five proton-active sites. Models with two proton binding sites yield significantly better fits to each of the titration datasets at each of the ionic strengths than models with only one site. However, models with three or more sites do not converge, indicating that they are underconstrained and that the data do not support a DLM with more than two sites. The averaged apparent proton binding constants, site densities, and V(Y) values for the best-fit *P. putida* and *P. mendocina* DLMs are compiled in Tables 1 and 2, respectively, and the average DLM fits (for the average of all the ionic strength data for each bacterium) are presented in Figs. 1 and 2, respectively.

Using the DLM approach to model the titration data yields pK<sub>a</sub> values for both bacteria that are strongly dependent upon ionic strength. For example, the pK<sub>a</sub> values for *P. mendocina* increase by more than a log unit from 2.1 to 3.3 (first site) and 4.8 to 6.8 (second site) as ionic strength increases from 0.01 to 0.5 M (Tables 1 and 2). The ap-

Table 2

Average non-electrostatic, DLM, and TLM proton binding stability constants and functional group site concentrations for triplicate *P. mendocina* titrations performed at three different ionic strengths

Ionic strength	$V(Y)$	Proton binding stability constants ( $pK_a$ )				Functional group site concentrations (mol/wet gram)				
		A	B	C	D	A	B	C	D	Total <sup>a</sup>
<i>Four-discrete-site non-electrostatic model</i>										
0.01 M										
Average	1.02	2.86	4.66	6.33	9.04	9.07E-5	1.11E-4	6.03E-5	5.13E-5	3.1E-4
Std. dev.	0.29	0.19	0.07	0.07	0.04	1.47E-5	2.38E-6	1.80E-6	1.24E-6	1.5E-5
0.1 M										
Average	0.33	3.42	4.74	6.51	9.25	9.58E-5	1.24E-4	5.08E-5	8.06E-5	3.5E-4
Std. dev.	0.09	0.11	0.11	0.12	0.11	1.54E-5	9.61E-6	3.04E-6	1.30E-5	2.3E-5
0.5 M										
Average	0.38	3.27	4.61	6.33	8.91	1.10E-4	1.28E-4	4.77E-5	7.93E-5	3.7E-4
Std. dev.	0.11	0.12	0.02	0.06	0.16	4.83E-6	1.29E-5	4.65E-6	1.01E-5	1.7E-5
<i>Two-site diffuse layer electrostatic model</i>										
0.01 M										
Average	5.48	2.10	4.79	NA	NA	2.21E-4	5.99E-5	NA	NA	2.8E-4
Std. dev.	1.39	0.08	0.15	NA	NA	2.50E-6	2.27E-6	NA	NA	3.4E-6
0.1 M										
Average	3.74	2.80	6.12	NA	NA	2.73E-4	7.18E-5	NA	NA	3.5E-4
Std. dev.	0.17	0.11	0.15	NA	NA	2.50E-6	2.27E-6	NA	NA	3.4E-6
0.5 M										
Average	4.37	3.31	6.75	NA	NA	2.69E-4	8.25E-5	NA	NA	3.5E-4
Std. dev.	1.05	0.05	0.28	NA	NA	8.92E-6	5.46E-6	NA	NA	1.0E-5
<i>Three-site triple-layer electrostatic model</i>										
0.01 M										
Average	2.03	1.44	2.53	5.20	NA	9.40E-5	1.29E-4	5.51E-5	NA	2.8E-4
Std. dev.	0.05	0.10	0.07	0.07	NA	2.61E-6	2.04E-6	1.61E-6	NA	3.7E-6
0.1 M										
Average	1.63	2.96	4.03	6.95	NA	1.60E-4	9.95E-5	7.97E-5	NA	3.4E-4
Std. dev.	0.37	0.32	0.44	0.40	NA	4.36E-5	2.57E-5	1.81E-5	NA	5.4E-5
0.5 M										
Average	1.41	3.22	4.09	7.11	NA	1.51E-4	1.22E-4	8.69E-5	NA	3.6E-4
Std. dev.	0.26	0.37	0.51	0.30	NA	2.44E-5	3.41E-5	1.08E-5	NA	4.3E-5

FITEQL was used to calculate  $pK_a$  values based on Eq. (2) in the text,  $K_a = [R-A_i^-]a_{H^+}/[R-A_iH^0]$ . NA, not applicable for model.

<sup>a</sup> Total functional group site concentrations.

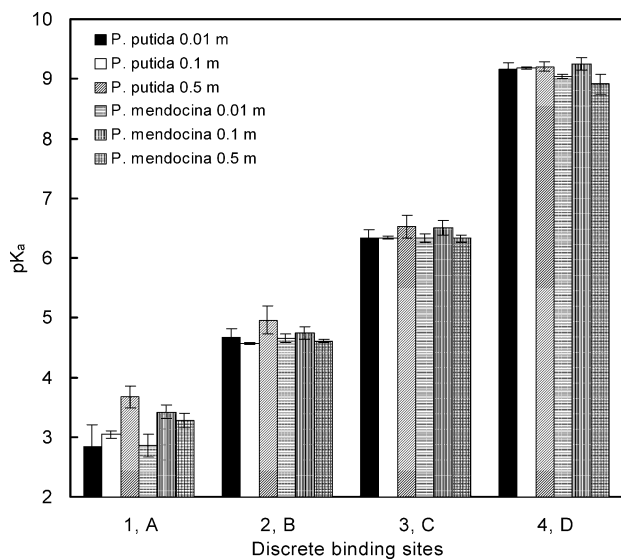


Fig. 3. Apparent proton binding stability constants ( $pK_a$ ) for *P. putida* and *P. mendocina* at ionic strengths of 0.01, 0.1, and 0.5 M. Error bars represent calculated  $1\sigma$  uncertainties based on modeling of three replicate titrations.

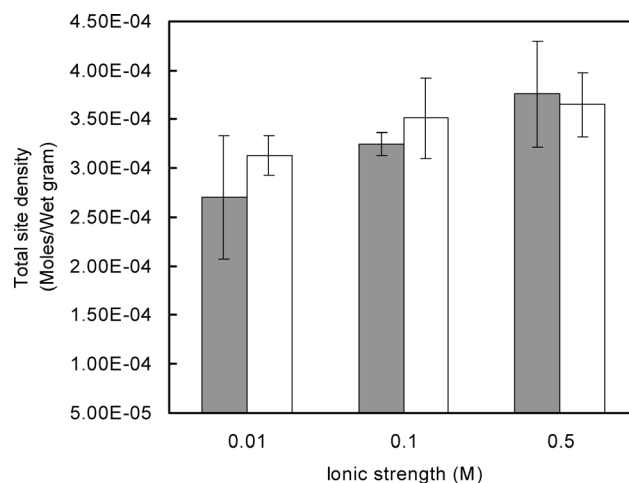


Fig. 4. Apparent total functional group site densities for *P. putida* (gray bars) and *P. mendocina* (clear bars) at ionic strengths of 0.01, 0.1, and 0.5 M. Error bars represent calculated  $1\sigma$  uncertainties based on modeling of three replicate titrations.

parent total site densities (the sum of the concentrations of the two binding sites developed using the DLM) for *P. putida* and *P. mendocina* are somewhat similar, but not within  $2\sigma$  uncertainties of each other, as compared at each ionic strength. The apparent total site densities for both bacteria also increase with increasing ionic strength using the DLM approach (Tables 1 and 2). The apparent site density for *P. putida* increases by about 60% over the ionic strength range of 0.01 to 0.5 M, while the apparent site density for *P. mendocina* increases by about 25% over the same ionic strength range (Tables 1 and 2).

The titration data were again remodeled, this time using the TLM approach for comparison to the non-electrostatic and DLM approaches. Because of the large number of adjustable parameters in the TLM, we began our analysis by setting  $C_1 = 1.2 \text{ F/m}^2$  and  $C_2 = 0.2 \text{ F/m}^2$ . These values were chosen because they are those commonly assumed in triple-layer models of mineral surfaces [37]. We systematically varied the number of discrete functional group sites and the cation stability constants ( $K_{\text{cation}}$ ) for each site, while allowing the  $\text{p}K_a$  and site density values to vary to best fit each dataset. We use this approach to constrain the number of discrete sites and the best-fit  $K_{\text{cation}}$  values for the 0.1 M data for each bacterium first, and then apply these values to determine if they can independently account for the remaining data collected at lower and higher ionic strengths for each bacterium separately. It was determined that a three-site model with  $\log K_{\text{cation}}$  values of  $-3.8$ ,  $-5.8$ , and  $-10.0$ , for the sites with the lowest to highest  $\text{p}K_a$  values, respectively, provided the best fit for both the *P. putida* and *P. mendocina* 0.1 M datasets. The  $C_1$ ,  $C_2$ , and  $K_{\text{cation}}$  values were then used as fixed parameters for the remainder of the modeling. The averaged apparent proton binding constants, site densities, and  $V(Y)$  values for the best-fit *P. putida* and *P. mendocina* models at each of the ionic strengths tested are compiled in Tables 1 and 2, respectively, and the average TLM model fits (for the average of all the ionic strength data for each bacterium) are presented in Figs. 1 and 2, respectively.

Like the DLM results and unlike the non-electrostatic model results, the TLM proton binding constant values for both bacteria are strongly dependent upon ionic strength. For example, the  $\text{p}K_a$  values for *P. mendocina* increase by more than a log unit from 1.4 to 3.2 (first site), 2.5 to 4.1 (second site), and 5.2 to 7.1 (third site), as ionic strength increases from 0.01 to 0.5 M. The  $\text{p}K_a$  results for *P. putida* exhibit similar variability. The apparent total site densities (the sum of the concentrations of binding sites for the three discrete sites) for *P. putida* and *P. mendocina* are again somewhat similar, but are not within  $2\sigma$  uncertainties of each other, as compared at each ionic strength. The apparent total site densities for both bacteria increase significantly with increasing ionic strength. The apparent total site density for *P. putida* increases by about 100% over the ionic strength range of 0.01 to 0.5 M, while the apparent total site density for *P. men-*

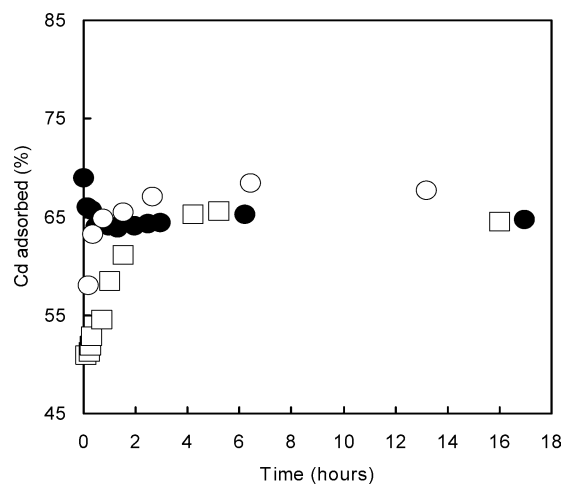


Fig. 5. Results from adsorption and desorption kinetics experiments conducted using *P. putida*. Closed circles (●) represent desorption results for pH 4.0. Open circles (○) represent adsorption results for pH 4.3. Open squares (□) represent duplicate adsorption results for pH 4.1.

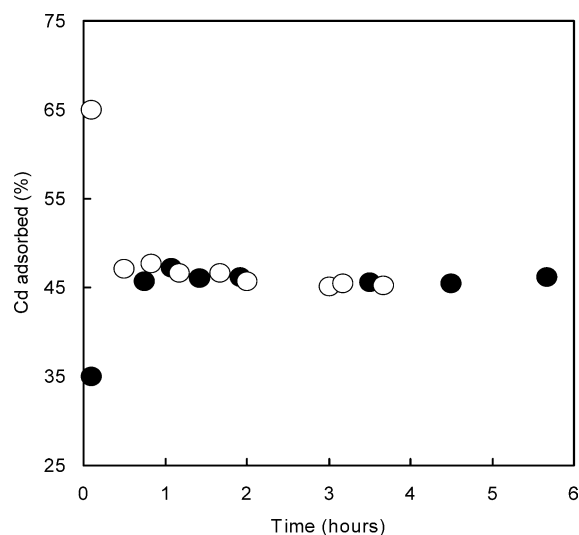


Fig. 6. Results from adsorption and desorption kinetics experiments conducted using *P. mendocina*. Closed circles (●) represent desorption results for pH 3.9. Open circles (○) represent adsorption results for pH 3.9.

*docina* increases by about 30% over the same ionic strength range.

#### 4.2. Cd adsorption/desorption kinetics

Adsorption/desorption kinetics data for *P. putida* and *P. mendocina* are presented in Figs. 5 and 6, respectively. The Cd desorption kinetics data for *P. putida* indicate that a steady-state extent of adsorption (at  $\text{pH} \sim 4.0$ ) occurs within about 30 min; however, the data from the Cd adsorption kinetics experiment using *P. putida* show that full adsorption takes about 4 h after an initial rapid ( $<30$  min) adsorption step. This trend of initial rapid Cd adsorption followed by slower Cd adsorption was confirmed in duplicate experiments (also shown in Fig. 5). Conversely, adsorption and

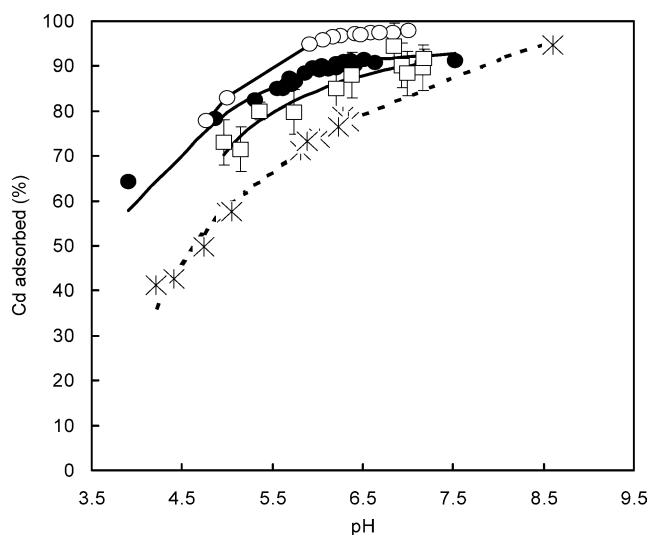


Fig. 7. Cd adsorption data for 10 g/L (○, 0.01 M ionic strength; ●, 0.1 M ionic strength; □, 0.5 M ionic strength) and 3 g/L (\*) *P. putida* experiments. All Cd adsorption experiments were conducted using 10 ppm Cd. The best non-electrostatic model fits for the individual 10 g/L datasets at each ionic strength are presented as solid curves, and the best model fit for the 3 g/L data is a dashed curve.

desorption of Cd occurred rapidly in the kinetics experiments using *P. mendocina*. A steady-state extent of adsorption (at  $\text{pH} \approx 3.9$ ) was reached in less than one hour in each experiment.

#### 4.3. Cd and Pb adsorption experiments

The concentrations of Cd adsorbed to the surfaces of *P. putida* and *P. mendocina* increase as a function of increasing pH, forming characteristic adsorption edges (Figs. 7 and 8, respectively). As expected, the adsorption edges for the experiments that used the largest bacteria:metal ratios occur at lower pH than those that used lower bacteria:metal ratios. The positions of the adsorption edges for the experiments conducted at 0.01, 0.1, and 0.5 M ionic strengths are roughly similar for each individual bacterial species. However, the final extent of Cd adsorption was consistently greatest in the 0.01 M experiments and was consistently least in the 0.5 M experiments. Data points below  $\text{pH} \sim 3.5$  are not shown or used in modeling calculations because metal adsorption results can be strongly influenced by damage to bacteria under acidic pH conditions (e.g., [24]), and ionic strength can vary considerably from the initial experimental values as the concentration of protons in solutions increases. Avoiding low pH data points in our study has no effect on the metal binding constants we develop; however, additional metal binding constants may be necessary to fully describe metal binding under acidic pH conditions. When compared at the same ionic strength and bacterial concentration, the Cd adsorption edges for *P. putida* occur at slightly lower pH than do those for *P. mendocina*. For example, 50% Cd uptake occurs at  $\text{pH} \sim 3.5$  for the 10 g/L (0.1 M) experiment using *P. putida*, while it occurs at  $\text{pH} 4.0$  for the 10 g/L (0.1 M) ex-

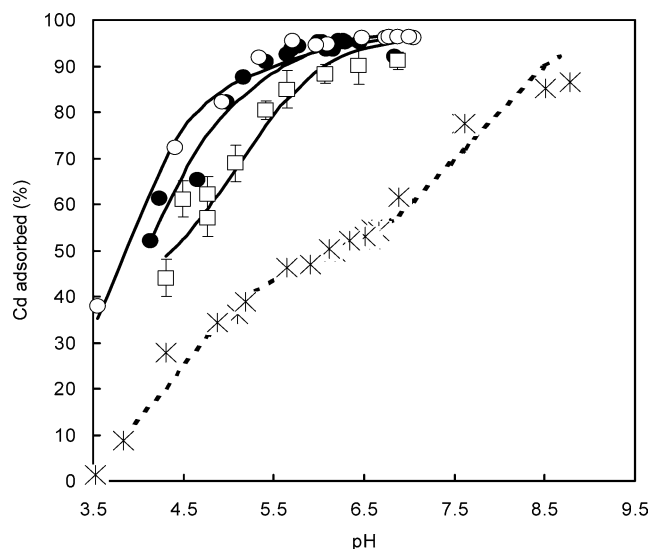


Fig. 8. Cd adsorption data for 10 g/L (○, 0.01 M ionic strength; ●, 0.1 M ionic strength; □, 0.5 M ionic strength) and 3 g/L (\*) *P. mendocina* experiments. All Cd adsorption experiments were conducted using 10 ppm Cd. The best non-electrostatic model fits for the individual 10 g/L datasets at each ionic strength are presented as solid curves, and the best model fit for the 3 g/L data is a dashed curve.

periment using *P. mendocina*. It was necessary to extrapolate the pH where 50% Cd uptake occurred in the *P. putida* experiment (Fig. 7). Hence, this value is associated with some uncertainty.

*P. putida* and *P. mendocina* exhibit Pb adsorption behavior that is similar to that observed for Cd in that adsorption increases with increasing pH and with increasing bacteria:metal ratio (Figs. 9 and 10, respectively). *P. putida* Pb adsorption results are similar to those for Cd in that the greatest extent of Pb adsorption occurs in the 0.01 M experiment. However, unlike the Cd data, the extents of Pb adsorption for *P. mendocina* are virtually indistinguishable for the 0.01, 0.1, and 0.5 M ionic strength experiments. Pb adsorption edges for *P. putida* and *P. mendocina* (both at 3 g/L bacteria) occurred at similar pH, reaching and maintaining maximum adsorption of about 90% total Pb adsorbed at approximately  $\text{pH} 5.0$ .

We model Cd adsorption data for *P. putida* and *P. mendocina* using a non-electrostatic approach to examine changes in apparent Cd binding constants in response to (1) changes in ionic strength at the same bacteria:metal ratio, and (2) changes in bacteria:metal ratio at the same ionic strength. To examine the effect of ionic strength, we constrain metal binding models using the average proton binding parameters developed through modeling of triplicate titrations (at each ionic strength for each bacterial species, see Tables 1 and 2). The best-fit metal binding models are determined by testing the fits of models involving metal binding onto any combination of the four deprotonated functional group sites. The apparent Cd binding constants and corresponding  $V(Y)$  values for all the best-fit models are compiled in Table 3.

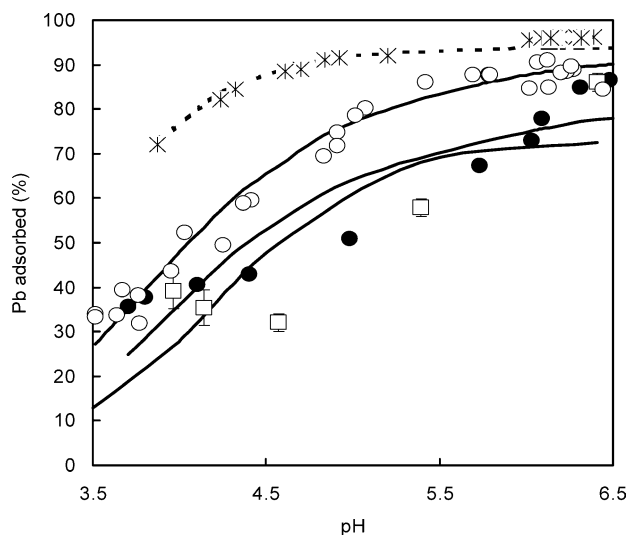


Fig. 9. Pb adsorption data for 1 g/L (○, 0.01 M ionic strength; ●, 0.1 M ionic strength; □, 0.5 M ionic strength) and 3 g/L (\*, 0.1 M ionic strength) *P. putida* experiments. All Pb adsorption experiments were conducted using 10 ppm Pb. The best non-electrostatic model fits for the individual 1 g/L datasets at each ionic strength are presented as solid curves, and the best model fit for the 3 g/L data is a dashed curve.

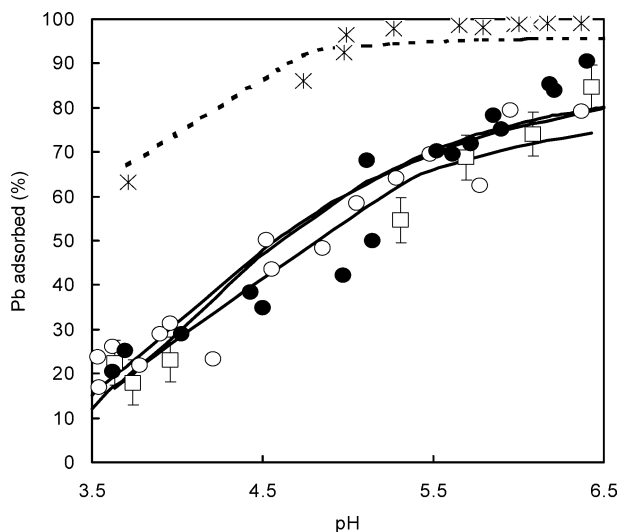


Fig. 10. Pb adsorption data for 0.5 g/L (○, 0.01 M ionic strength; ●, 0.1 M ionic strength; □, 0.5 M ionic strength) and 3 g/L (\*, 0.1 M ionic strength) *P. mendocina* experiments. All Pb adsorption experiments were conducted using 10 ppm Pb. The best non-electrostatic model fits for the individual 0.5 g/L datasets at each ionic strength are presented as solid curves, and the best model fit for the 3 g/L data is a dashed curve.

The best-fit models for Cd adsorption onto 10 g/L *P. putida* at all ionic strengths involve the complexation of Cd with the deprotonated forms of sites 2 and 3. The best-fit models for Cd adsorption onto 10 g/L *P. mendocina* at all ionic strengths are identical in that they involve the complexation of Cd with the deprotonated forms of sites B and C. Binding onto the lowest  $pK_a$  sites was not necessary to fit the *P. putida* or *P. mendocina* data because low-pH data points ( $pH < 3.5$ ) are not included as part of this analysis (see dis-

Table 3

Log apparent Cd binding stability constants for best-fit non-electrostatic adsorption models for 10 g/L *P. putida* and *P. mendocina* experiments conducted at 0.01, 0.1, and 0.5 M ionic strengths and for 3 g/L *P. putida* and *P. mendocina* experiments conducted at 0.1 M ionic strength

Bacterium and ionic strength	$V(Y)$	Site 1	Site 2	Site 3	Site 4
<i>P. putida</i>					
0.01 M (10 g/L)	0.10	NA	3.77	5.30	NA
0.1 M (10 g/L)	2.44	NA	4.27	4.08	NA
0.5 M (10 g/L)	1.65	NA	4.26	4.74	NA
0.1 M (3 g/L)	1.48	NA	4.17	4.82	6.21
<i>P. mendocina</i>					
0.01 M (10 g/L)	0.84	Site A	Site B	Site C	Site D
0.1 M (10 g/L)	2.55	NA	4.00	5.40	NA
0.5 M (10 g/L)	6.29	NA	3.40	5.30	NA
0.1 M (3 g/L)	4.45	NA	3.84	3.73	5.90

FITEQL was used to calculate stability constants based on Eq. (4) in text,  $K = [R-A_i(M)^+]/a_{M^{2+}}[R-A_i^-]$ .

cussion above). The best fitting model for each dataset is presented with the adsorption data in Figs. 7 and 8.

Next, we use the non-electrostatic approach to model the 3 g/L:10 ppm Cd datasets for the 0.1 M ionic strength systems for each bacterium. The best-fit Cd binding models are determined as described above, and the apparent Cd binding constants and corresponding  $V(Y)$  values for the best-fit 3 g/L models are compiled in Table 3. The best-fit models for Cd adsorption onto 3 g/L *P. putida* and *P. mendocina* at 0.1 M ionic strength involve the complexation of Cd with the deprotonated forms of sites 2, 3, and 4 and sites A, B, and C, respectively. These models are different from the 10 g/L models in that Cd binding onto site 4 (site D for *P. mendocina*) is additionally necessary to account for the adsorption data at the highest pH. The best-fit models for the 3 g/L *P. putida* and *P. mendocina* experiments are presented as dashed curves in Figs. 7 and 8, respectively.

We model Pb adsorption onto *P. putida* and *P. mendocina* in the same fashion as the Cd adsorption datasets. The 0.01, 0.1, and 0.5 M datasets collected from the 1 g/L *P. putida* and 0.5 g/L *P. mendocina* experiments are modeled first to examine the effect of ionic strength on apparent Pb binding constants. The best-fit models for Pb adsorption onto 1 g/L *P. putida* at ionic strengths of 0.01 and 0.1 M involve the complexation of Pb with the deprotonated forms of sites 2 and 3. Complexation of Pb with site 2 alone was necessary to best fit the 1 g/L *P. putida* data at an ionic strength of 0.5 M. The best-fit models for Pb adsorption onto 0.5 g/L *P. mendocina* at all ionic strengths are identical in that they involve the complexation of Pb with the deprotonated forms of sites B and C. The apparent Pb binding constants and corresponding  $V(Y)$  values for the best-fit models are compiled in Table 4, and the model fits for each dataset are presented with the raw data in Figs. 9 and 10. The best-fit models for Pb (10 ppm) adsorption onto 3 g/L *P. putida* and onto 3 g/L *P. mendocina* at 0.1 M ionic strength each involve the complexation of Pb with the deprotonated form of site 2 (or

Table 4

Log apparent Pb binding stability constants for best-fit non-electrostatic adsorption models for 1 g/L *P. putida* and 0.5 g/L *P. mendocina* experiments conducted at 0.01, 0.1, and 0.5 M ionic strengths and for 3 g/L *P. putida* and *P. mendocina* experiments conducted at 0.1 M ionic strength

Bacterium and ionic strength	$V(Y)$	Site 1	Site 2	Site 3	Site 4
<i>P. putida</i>					
0.01 m (1 g/L)	2.24	NA	5.04	5.60	NA
0.1 m (1 g/L)	11.2	NA	4.85	5.14	NA
0.5 m (1 g/L)	29.8	NA	4.90	NA	NA
0.1 m (3 g/L)	0.31	NA	5.14	NA	NA
<i>P. mendocina</i>					
		Site A	Site B	Site C	Site D
0.01 m (0.5 g/L)	5.30	NA	4.94	5.60	NA
0.1 m (0.5 g/L)	8.12	NA	5.12	6.20	NA
0.5 m (0.5 g/L)	7.38	NA	5.08	6.20	NA
0.1 m (3 g/L)	1.38	NA	5.27	NA	NA

FITEQL was used to calculate stability constants based on Eq. (4) in text,  $K = [R-A_i(M)^+]/a_{M^{2+}}[R-A_i^-]$ .

site B) only. The apparent Pb binding constants for the 3 g/L data are also compiled in Table 4, and the best-fit model curves are presented in Figs. 9 and 10.

#### 4.4. Cd, Pb, and Sr isotherm experiments

In this set of experiments, the pH of each batch reaction vessel for each isotherm experiment was held constant, while the ionic strength of each vessel was manipulated. The pH for the Cd, Pb, and Sr isotherm experiments averaged  $5.9 \pm 0.2$ ,  $5.5 \pm 0.2$ , and  $6.3 \pm 0.2$ , respectively, for both bacterial species. The ionic strength of each reaction vessel ranged from 0.001 to  $\sim 0.6$  M. The extents of Cd, Pb, and Sr adsorption that we observed for each bacterial species decreased as a function of increasing ionic strength, forming a gently dipping series of data points when plotted on a log scale (Figs. 11, 12, and 13 for each of the metals, respectively). The ionic strength effects on the extent of Cd and Pb adsorption as a function of ionic strength are similar in magnitude, and are similar for both bacterial species tested. Conversely, the magnitude of the changes in the extents of Sr adsorption from low to high ionic strength are similar for each bacterium, but are much greater in magnitude than we observed in the Cd and Pb experiments. For example, the amount of adsorbed Cd and Pb changes by about 20% over the ionic strength range of 0.001 to 0.6 M, while the amount of adsorbed Sr changes by more than 40% over this same ionic strength range.

We model each ionic strength isotherm using the non-electrostatic approach, as described above for the adsorption edge data; however, we additionally input the ionic strength of the electrolyte solution at each experimental point as serial data in our models. The average of the proton binding constants and site densities for all three ionic strengths (for each bacterium separately) were used as input to constrain the ionic strength isotherm models. We chose to calculate best-fitting Cd/Pb binding constants for metal complexation

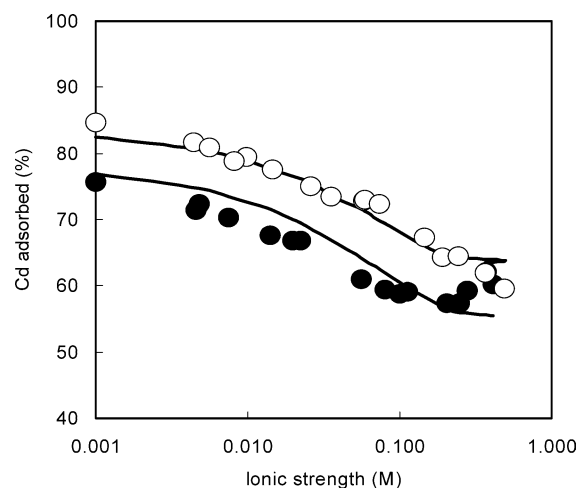


Fig. 11. Cd adsorption isotherm data for 3 g/L *P. putida* (●) and 3 g/L *P. mendocina* (○) at constant pH ( $5.9 \pm 0.2$ ), constant total Cd concentration (10 ppm), and variable ionic strength (0.001 to 0.6 M). The best non-electrostatic model fits for each dataset, constrained for Cd binding onto site 2 for *P. putida* and site B for *P. mendocina*, are presented as solid curves.

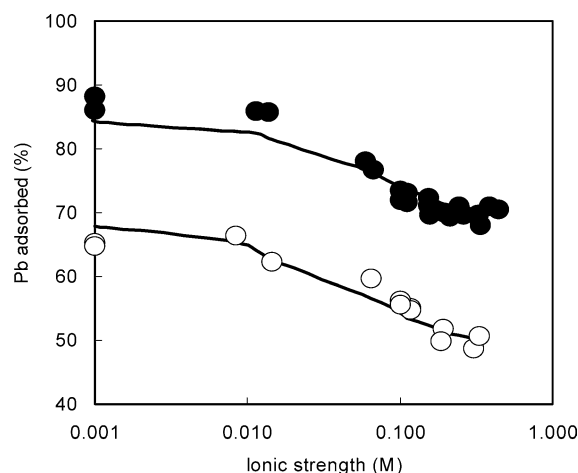


Fig. 12. Pb adsorption isotherm data for 1 g/L *P. putida* (●) and 1 g/L *P. mendocina* (○) at constant pH ( $5.5 \pm 0.2$ ), constant total Pb concentration (10 ppm), and variable ionic strength (0.001 to 0.6 M). The best non-electrostatic model fits for each dataset, constrained for Pb binding onto site 2 for *P. putida* and site B for *P. mendocina*, are presented as solid curves.

with site 2/B only, and best-fitting Sr binding constants for complexation with site 3/D only (the site with a higher  $pK_a$  was chosen because the equilibrium pH for these experiments was higher than those for the Pb and Cd experiments). By utilizing this approach, we can determine the degree to which a non-electrostatic model is capable of describing the observed changes in ionic strength. Because this model does not account for changes in the bacterial surface electric field, and the experiments were conducted at a constant pH and total metal concentration, only changes in the activity coefficient of the metal cation (as a function of ionic strength) can influence in the shape of the best-fit curve for each experiment.

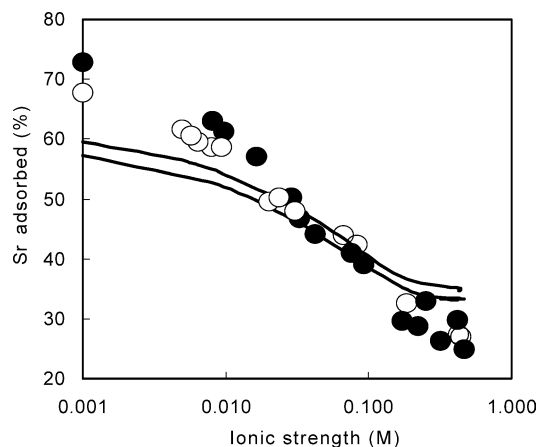


Fig. 13. Sr adsorption isotherm data for 6 g/L *P. putida* (●) and 6 g/L *P. mendocina* (○) at constant pH ( $6.3 \pm 0.2$ ), constant total Sr concentration (10 ppm), and variable ionic strength (0.001 to 0.6 M). The best non-electrostatic model fits for each dataset, constrained for Sr binding onto site 3 for *P. putida* and site C for *P. mendocina*, are presented as solid curves.

Model fits for both the Cd and Pb datasets are in excellent agreement with the observed extents of adsorption over the entire ionic strength range of the experiments (Figs. 11 and 12). For example, the  $V(Y)$  values for Pb and Cd complexation with site B of *P. mendocina* are 0.8 and 0.6, respectively, and  $V(Y)$  values are 3.7 and 0.4 for Pb and Cd complexation with site 2 of *P. putida*, respectively. The calculated log apparent Cd binding constants for *P. putida* and *P. mendocina* are both 4.3, while the best-fit log apparent Pb binding constants for these bacteria are 5.0 and 5.2, respectively. The binding constants constrained by modeling the ionic strength isotherms agree remarkably well with those developed independently by modeling adsorption edge data. For example, the log Cd binding constants for site 2 of *P. putida* and site B of *P. mendocina* that were constrained from adsorption edge data ranged from 3.8 to 4.3 and from 3.4 to 4.0, respectively, for experiments conducted at 0.01, 0.1, and 0.5 M ionic strength (Table 3). The log Pb binding constants for site 2 of *P. putida* and site B of *P. mendocina* that were constrained from adsorption edge data ranged from 4.9 to 5.0 and from 4.9 to 5.1, respectively (Table 4).

Best-fit models for the Sr datasets are not capable of fitting the data over the entire ionic strength range tested (Fig. 13). Hence, the model fits result in a larger  $V(Y)$  value of 24.8 for complexation with site 3 of *P. putida* and a  $V(Y)$  value of 15.2 for complexation with site C of *P. mendocina*. Log binding constant values for Sr complexation are 4.2 for both bacterial species. Best-fit models are presented as solid curves for each dataset in Figs. 11, 12, and 13.

We test whether the DLM approach provides a better fit to the Sr isotherms than the non-electrostatic model. However, the required input for the DLM approach within FITEQL requires that a single concentration value be entered for the symmetrical electrolyte. Hence, we cannot model the entire ionic strength isotherm dataset as a single unit, inputting

ionic strength as serial data, as was done previously using the non-electrostatic approach. Instead, we are forced to compare DLM and non-electrostatic approaches by modeling each individual data point within each Sr binding dataset separately. We use this approach to calculate the specific Sr binding constant that is necessary to perfectly fit each individual data point. In this fashion, we calculate different values of the Sr binding constant for each data point, and we compare the effectiveness of each modeling approach by calculating the standard deviation associated with the average calculated Sr binding constant value developed using the DLM and non-electrostatic approaches. The model that has the least variability (smallest standard deviation) in binding constant values over the entire ionic strength range, is the model that best fits the dataset. As with the non-electrostatic models, we use the average DLM proton binding and site density parameters for all three ionic strengths (for each bacterium separately) to constrain Sr binding constants. We choose to constrain Sr binding constants for complexation with the second (higher  $pK_a$ ) site of the DLM. The results of this modeling demonstrate that log binding constant values for Sr binding developed using the DLM approach average 2.0 with a  $1\sigma$  uncertainty of 0.6 for the *P. putida* Sr dataset, and average 0.9 with a  $1\sigma$  uncertainty of 0.7 for the *P. mendocina* Sr dataset. The log binding constant values for Sr binding developed using the non-electrostatic approach average 4.2 with a  $1\sigma$  uncertainty of 0.1 for the *P. putida* Sr dataset, and average 4.2 with a  $1\sigma$  uncertainty of 0.1 for the *P. mendocina* Sr dataset.

## 5. Discussion

### 5.1. Proton adsorption behavior and ionic strength

Although there are measurable changes in the shapes of the *P. putida* and *P. mendocina* titration curves as a function of ionic strength (Figs. 1 and 2), non-electrostatic modeling results demonstrate that ionic strength has a small or negligible effect on proton binding constants over the tested ionic strength range of 0.01 to 0.5 M. Apparent total site densities for each bacterium increase with increasing ionic strength by about 40% for *P. putida* and about 20% for *P. mendocina*. Similar increases in total site density with increasing ionic strength are reported by Daughney and Fein [13] for the Gram positive bacterial species *B. subtilis* and *B. licheniformis*, and by Cox et al. [9] for *B. subtilis*. Martinez et al. [10] observed a similar trend for the Gram negative bacterial species, *E. coli*, in that apparent total site densities increased by about 20% from 0.01 to 0.05 M ionic strength, but remained the same between 0.05 and 0.5 M ionic strength. Although there are a limited number of studies available for comparison, it appears that the ionic strength effects for protonation reactions on bacterial surfaces are ‘universal’ in that they affect different Gram positive and Gram negative bacterial species similarly. Martinez et al. [10] describe

an exception to this observation, by showing that under the conditions of their study the apparent total site density for *B. subtilis* first went up slightly from 0.01 to 0.05 M ionic strength, but then decreased slightly when ionic strength was increased to 0.5 M.

The four-site non-electrostatic surface complexation model developed in our study not only fits the titration data reasonably well at each ionic strength, but the effect of ionic strength on apparent proton binding constants and site densities is relatively small. For example, the magnitude of the observed differences in apparent total site density over the tested ionic strength range is similar to the  $2\sigma$  errors calculated from triplicate titration experiments at each individual ionic strength. Equivalent model fits to the titration datasets at each ionic strength can be achieved using the DLM or TLM treatments (Figs. 1 and 2). However, the effect of ionic strength on the intrinsic DLM and TLM proton binding constants and site densities is large, and is much greater than the effect of ionic strength on the apparent stability constants developed using the non-electrostatic approach.

Because the effect of ionic strength on protonation reactions on the bacterial surface is small, the DLM and TLM approaches significantly overpredict the magnitude of electrostatic corrections necessary to describe these reactions. Overprediction of the diffuse-layer potential using the DLM has been demonstrated previously at high ionic strengths for mineral surfaces [39]; however, the TLM has been successfully applied for modeling protonation reactions on mineral surfaces at ionic strengths greater than those tested in this study [37]. Careful comparison of the magnitude of electrostatic effects on raw titration data from bacterial surfaces and mineral surfaces (data compiled by Sahai and Sverjensky [37]) suggests that the shapes and positions of titration data change more for mineral surfaces than for bacterial surfaces in response to equal changes in salt concentration. For example, at pH 6.0, the charge on the surface of *P. putida* changes by about  $0.025 \text{ C/m}^2$  over the ionic strength range of 0.01 to 0.5 M, while the charge on corundum and goethite change by about  $0.05 \text{ C/m}^2$  at the same pH over a similar ionic strength range [37]. This suggests that the electrostatic treatments developed for mineral surfaces cannot be directly applied to bacterial surfaces, because the surface charges for bacteria and mineral surfaces change disproportionately as a function of ionic strength. This result is not entirely surprising because the bacterial surface is not actually a ‘surface’ but a three-dimensional fabric of organic polymers. In contrast, the changes in protonation behavior for humic and fulvic acids as a function of salt concentration appear to be similar to those observed for bacterial surfaces. The shapes and positions of titration curves for most humic and fulvic acids change in similar ways and in similarly small magnitudes to those of bacterial surfaces as a function of ionic strength (see compilation by Milne et al. [40]). Using a similar four-site non-electrostatic surface complexation model to that developed in this study, Borrok and Fein [41] show that the ionic strength effects on proton binding for a variety of humic and

fulvic acids (over the range of 0.01 to 0.3 M) is rather small, and of similar magnitude to that described for the bacterial surfaces in this study. Hence, for most modeling applications, it may be reasonable to employ a similar discrete site surface complexation model, neglecting the effect of ionic strength on proton binding onto bacterial surfaces and dissolved humic substances.

## 5.2. Metal adsorption/desorption kinetics

Our results demonstrate that different Gram negative bacterial species can exhibit significantly different metal adsorption and desorption reaction kinetics. The rapid adsorption and desorption of Cd onto *P. mendocina* are similar to the rate of adsorption and desorption previously observed for Cd binding to *B. subtilis* [8] and for Zn adsorption onto the Gram negative bacterium from the genus *Enterobacteriaceae* [15]. However, the two-step, 4-h adsorption process observed for Cd binding onto *P. putida* is most similar to that previously observed for Cd adsorption onto *E. coli* [14]. It is unclear whether differences in the kinetics of Cd adsorption are related to real differences in binding (perhaps onto different portions of the Gram negative cell membrane), or whether these differences are triggered by structural changes brought about by exposure to acidic solutions during the adsorption kinetics experiments [23]. This may explain why the desorption experiments, which begin at neutral pH, provided similar results for both bacteria. Clearly, spectroscopic information would be necessary to confirm any proposed mechanism.

## 5.3. Cd, Pb, and Sr adsorption and ionic strength effects

Under identical experimental conditions, the Gram negative bacteria tested in this study adsorb Cd to roughly similar extents, but to greater extents than individual Gram positive bacterial species [23] or consortia of bacterial species that include Gram positive bacteria [11]. The extents of Pb and Sr adsorption in our study are also similar for *P. putida* and *P. mendocina*. However, these results are not directly comparable to previous studies, because previous studies examining Pb and Sr utilized acid-treated bacteria (e.g., [8]).

As ionic strength increases from 0.01 to 0.5 M, the extent of Cd and Pb adsorption onto *P. putida* and *P. mendocina* decreases slightly in both the adsorption edge (Figs. 7 and 8, respectively, for Cd and Figs. 9 and 10, respectively, for Pb) and adsorption isotherm experiments (Fig. 11 for Cd and Fig. 12 for Pb). The observed decreases in Cd and Pb adsorption with increasing ionic strength can be attributed to one or more of the following factors: (1) enhanced competition of the background electrolyte cation ( $\text{Na}^+$ ) for deprotonated binding sites at high ionic strength, (2) changes in the accessibility (or ‘activity’) of the metal binding functional group sites on the bacterial surfaces as a function of ionic strength (e.g., [19]), or (3) changes in the activity of the aqueous metal cations as a function of ionic strength.

Non-electrostatic modeling results from the Cd and Pb adsorption experiments support the third possibility. The fact that a modeling approach that does not account for electric field interactions ('non-electrostatic') can be used to successfully fit data from the Cd and Pb ionic strength isotherm experiments, strongly suggests that changes in the activity of the aqueous metal cation control the observed adsorption behavior. In other words, a bacterial surface electric field model is not necessary to provide an adequate fit to the Cd and Pb adsorption data for *P. putida* and *P. mendocina* over the ionic strength range tested in our study. This is further illustrated in the similarity of the non-electrostatic binding constant values calculated from the adsorption edge data at ionic strengths of 0.01, 0.1, and 0.5 M. Apparent Cd binding constants change by only about 0.5 log units over this ionic strength range for both *P. putida* and *P. mendocina* (Table 3). Apparent binding constants for Pb change by only about 0.2 log units for site 2 of *P. putida* and site B of *P. mendocina* over this ionic strength range (Table 4). These differences in apparent binding constants are not statistically meaningful because variability of  $\pm 0.2$  log units is common when comparing binding constants constrained using data collected from two identical experiments or data from experiments conducted under identical conditions with variable bacteria:metal ratios. Equilibrium constants for surface complexation reactions should be valid over a range of bacteria:metal ratios as long as the adsorption mechanisms remain constant. For this reason, we expect the apparent Cd binding constants for Cd adsorption edge experiments conducted using 10 and 3 g/L bacteria at 0.1 M ionic strength to be equal. Instead, we observe a change of about 0.2 log units in apparent Cd binding constants for each bacterium (Table 3). Apparent Pb binding constants for Pb adsorption edge experiments conducted using 3 and 1 g/L *P. putida* also change by about 0.2 log units, while apparent Pb binding constants constrained from the 3 and 0.5 g/L *P. mendocina* adsorption edge experiments change by about 0.4 log units (Table 4). These variations are caused either from experimental uncertainties or from real variations in the binding mechanisms between the two bacterial concentration conditions. This variation establishes the degree of uncertainty involved in application of a surface complexation model under constant ionic strength conditions. Hence, we conclude that ionic strength effects on apparent Cd and Pb binding constants over the range of 0.01 to 0.5 M ionic strength are small, and of similar magnitude to the experimental uncertainty associated with their development. Furthermore, because the calculated apparent binding constants for Cd and Pb are relatively invariant as a function of ionic strength, it may suggest that Cd and Pb are primarily adsorbed to the surfaces of *P. putida* and *P. mendocina* as inner sphere complexes under the conditions of our study. Application of the DLM and TLM models to the Cd and Pb datasets (data not presented) resulted in poorer fits and dramatic variability in intrinsic stability constants over the tested ionic strength range. Hence, the DLM and

TLM electrostatic treatments greatly overpredict the effect of ionic strength for proton, Cd, and Pb adsorption.

In contrast to the Cd and Pb adsorption data, a non-electrostatic modeling approach is not capable of fitting Sr ionic strength isotherm data over the entire ionic strength range tested. This suggests that in addition to the effects caused by changes in the activity of the aqueous metal cation, one or both of the remaining electrostatic factors outlined above control the observed adsorption behavior for Sr. This may also suggest that Sr is primarily adsorbed to the surfaces of *P. putida* and *P. mendocina* as an outer sphere complex (a hypothesis supported by Small et al. [21] and Yee et al. [17] for *S. alga* and *B. subtilis*, respectively). Despite the greater effect of salt concentration, the Sr stability constants developed using the non-electrostatic model (for each data point individually) are more consistent than those developed using the DLM. That is, the standard deviation in apparent Sr binding constants calculated for each Sr adsorption data point is only 0.1 log unit for both *P. putida* and *P. mendocina*, while the standard deviations of intrinsic Sr binding constants calculated using the DLM are 0.6 and 0.7 log units for each bacterium, respectively. The DLM greatly overpredicts the effect of ionic strength on Sr adsorption over the entire tested range (0.001 to 0.5 M), but also over smaller ranges of the data under low ionic strength conditions (i.e., 0.001 to 0.01 M). Application of the TLM to the Sr isotherm data produced similarly poor results to those of the DLM, and are not discussed further here.

The effects of ionic strength on Cd and Pb binding onto the bacterial surfaces documented in our study are generally similar to those observed for Cd and Pb binding onto the surface of *B. subtilis* [13]. However, in the Daughney and Fein study [13], the Gram positive bacterium, *B. licheniformis*, exhibited opposite, 'promotive,' behavior in that the extent of Cd adsorption increased with increasing ionic strength. The reasons for this difference remain unclear, but could be related to the specific experimental conditions tested. The effects of ionic strength on Cd and Pb binding onto *P. putida* and *P. putida* are also similar to those determined for adsorption of these metals onto a host of mineral surfaces, including iron oxides [42–44], calcite [45,46], and clay minerals [47,48]. The extents of Cd adsorption onto the mineral surfaces in these studies was only weakly affected by changes in ionic strength, while the extents of Pb adsorption remained unaffected by changes in ionic strength in all the studies. The effects of ionic strength on Sr binding onto bacterial surfaces in this study and in previous studies by Ledin et al. [19] and Small et al. [21] for *P. putida* and *S. alga*, respectively, are similar and appear to be greater than those observed for Sr binding onto some mineral surfaces [21]. The effect of ionic strength on Cd and Pb binding onto natural organic macromolecules like humic and fulvic acids [49,50] appears to be more pronounced than that observed in our study for bacterial surfaces or than that observed in studies of mineral surfaces. For example, Liu and Gonzalez [50] suggest that the dramatic changes in the extents of Cd and Pb adsorp-

tion onto Aldrich humic acid over the ionic strength range of 0.02 to 0.8 M are due to electrostatic effects; however, they do not separate activity coefficients effects from bacterial surface electric field effects. The adsorption of Sr onto natural organic matter has not been investigated sufficiently as a function of ionic strength, and therefore cannot be compared to the results in our study. These observations may suggest that changes in the behavior of metal adsorption onto bacterial surfaces in response to changes in ionic strength are intermediate in magnitude when compared to those associated with mineral surfaces and dissolved humic substances.

## 6. Summary and conclusions

This study is the first to examine the proton and metal (Cd, Pb, and Sr) adsorption behavior of Gram negative bacterial species over a broad range of ionic strength (0.001 to 0.6 M). Results suggest that proton binding behavior is only moderately influenced by changes in ionic strength and, at least for some applications, can be adequately described using a four-discrete-site non-electrostatic surface complexation model. DLM or TLM treatments not only fail to improve model fits for proton binding datasets, but also significantly overpredict the effect of ionic strength on proton binding, resulting in intrinsic binding constants that change by more than an order of magnitude over the ionic strength range of 0.01 to 0.5 M.

The extents of Cd and Pb adsorption onto *P. putida* and *P. mendocina* decrease slightly as ionic strength increases. However, this decrease can be entirely attributed to changes in the activity of the aqueous metal cation as a function of ionic strength and not to bacterial surface electric field interactions. As with the proton binding data, a four-discrete-site non-electrostatic surface complexation model is adequate for describing Cd and Pb binding onto the Gram negative bacterial species tested under the experimental conditions in this study. Moreover, the DLM and TLM electrostatic treatments are not only unnecessary, but result in poor fits to the data with more variability in calculated binding constants. The extent of Sr adsorption decreases more dramatically than Cd or Pb adsorption as a function of increasing ionic strength, demonstrating that bacterial surface electric field interactions play a significant role in the observed Sr adsorption behavior. However, despite the clear influence of the electric double layer on Sr adsorption, the four-discrete-site non-electrostatic SCM was more accurate in describing the Sr adsorption data over the entire ionic strength range than either the DLM or TLM electrostatic treatments.

Inspection of our results and comparison to results from previous studies leads to the following conclusions: (1) the effect of ionic strength on apparent proton, Cd, and Pb binding constants, and apparent site densities for bacterial surfaces is small, and is similar in magnitude to the  $2\sigma$  experimental uncertainties; (2) both Cd and Pb form strong chemical bounds (likely inner sphere complexes) with the

surfaces of the tested Gram negative bacterial species, while Sr forms electrostatic bonds (likely outer sphere complexes); (3) under the conditions of this study, reasonable approximations of proton, Cd, Pb (and possibly Sr) adsorption behavior can be obtained by models that neglect bacterial surface electric field effects; (4) the ionic strength effects that are observed in our study appear to be similar for different Gram negative and Gram positive bacterial species, suggesting that electric field interactions for bacterial surfaces may be ‘universal’; and (5) the protonation framework and geometric environment of the functional groups on the bacterial surface are strikingly different from those of a mineral surface, and this is likely why traditional DLM and TLM electrostatic treatments fail to successfully describe electrostatic interactions with the bacterial surface.

Because the effect of ionic strength on proton and metal adsorption reactions onto bacterial surfaces is small, a simplified, non-electrostatic surface complexation model like the one developed here may be the most functional predictive modeling tool for accounting for bacterial surface adsorption in complex environments. The uncertainties associated with application of purely mechanistic surface complexation models to multi-component, heterogeneous systems is large because it is impossible to delineate the exact types (i.e., mineral surfaces, organic acids, bacterial surfaces, etc.) and abundances of surface functional group sites available for adsorption [41,51]. Mainly because of this difficulty, simplified, semi-empirical surface complexation modeling approaches have been developed for describing adsorption reactions in realistic geologic settings [51–55]. The results from our study suggest that it may be reasonable to neglect bacterial surface electric field effects for bacterial surfaces when applying these simplified surface complexation models to geologic systems. Using this approach, stability constants for Sr and other weakly adsorbing cations can be estimated using a non-electrostatic modeling approach for each specific ionic strength range of interest.

## Acknowledgments

Research funding was provided by the National Science Foundation through Grant EAR02-07169 and the Environmental Molecular Science Institute Grant EAR02-21966. The Department of Energy, Division of Basic Energy Sciences, also provided partial funding. D.B. was partially supported through a University of Notre Dame Arthur J. Schmitt Presidential Fellowship. Some aqueous Cd analyses were conducted at the Center for Environmental Science and Technology at the University of Notre Dame. ICP–MS analyses were conducted by Jinesh Jain at the University of Notre Dame’s ICP–MS Analytical Research Facility. We thank Larry Hersman for providing us with the original culture of *Pseudomonas mendocina*, and we appreciate the comments of two reviewers, which significantly improved the manuscript.

## References

- [1] M.D. Mullen, D.C. Wolf, F.G. Ferris, T.J. Beveridge, C.A. Flemming, G.W. Bailey, *Appl. Environ. Microbiol.* 55 (1989) 3143–3149.
- [2] T.J. Beveridge, *Annu. Rev. Microbiol.* 43 (1989) 147–171.
- [3] S.M. Barns, S.A. Nierzwicki-Bauer, in: J.F. Banfield, K.H. Nealson (Eds.), *Geomicrobiology: Interactions Between Microbes and Minerals*, in: *Rev. Mineral.*, vol. 35, Mineralogical Society of America, 1997, pp. 35–79.
- [4] T.G. Tornabene, H.W. Edwards, *Science* 176 (1972) 1334–1335.
- [5] P.D. Tortell, M.T. Maldonado, J. Granger, N.M. Price, *FEMS Microbiol. Ecol.* 29 (1999) 1–11.
- [6] R.W. Harvey, J.O. Leckie, *Mar. Chem.* 15 (1985) 333–344.
- [7] C.C. Plette, W.H. Van Riemsdijk, M.F. Benedetti, A. Van der Wal, *J. Colloid Interface Sci.* 173 (1995) 354–363.
- [8] J.B. Fein, C.J. Daughney, N. Yee, T.A. Davis, *Geochim. Cosmochim. Acta* 61 (1997) 3319–3328.
- [9] J.S. Cox, D.S. Smith, L.A. Warren, F.G. Ferris, *Environ. Sci. Technol.* 33 (1999) 4514–4521.
- [10] R.E. Martinez, D.S. Smith, E. Kulczycki, F.G. Ferris, *J. Colloid Interface Sci.* 253 (2002) 130–139.
- [11] D. Borrok, J.B. Fein, C.F. Kulpa, *Geochim. Cosmochim. Acta* 68 (2004) 3231–3238.
- [12] A. van der Wal, W. Norde, A.J.B. Zehnder, J. Lyklema, *Colloids Surf. B Biointerfaces* 9 (1997) 81–100.
- [13] C.J. Daughney, J.B. Fein, *J. Colloid Interface Sci.* 198 (1998) 53–77.
- [14] N. Yee, J.B. Fein, *Geochim. Cosmochim. Acta* 65 (2001) 2037–2042.
- [15] B.T. Ngwenya, I.W. Sutherland, L. Kennedy, *Appl. Geochem.* 18 (2003) 527–538.
- [16] J.R. Haas, *Chem. Geol.* 209 (2004) 67–81.
- [17] N. Yee, D.A. Fowle, F.G. Ferris, *Geochim. Cosmochim. Acta* 68 (2004) 3657–3664.
- [18] J.H.A.M. Wonders, H.P. Vanleeuwen, J. Lyklema, *J. Colloids Surf. A* 120 (1997) 221–233.
- [19] M. Ledin, K. Pedersen, B. Allard, *Water Air Soil Pollut.* 93 (1997) 367–381.
- [20] J.R. Haas, T.J. Dichristina, *Chem. Geol.* 180 (2001) 33–54.
- [21] T.D. Small, L.A. Warren, F.G. Ferris, *Appl. Geochem.* 16 (2001) 939–946.
- [22] L. Hersman, A. Huang, P. Maurice, J. Forsythe, *Geomicrobiol. J.* 17 (2000) 1–13.
- [23] D. Borrok, J.B. Fein, M. Tischler, E. O’Loughlin, H. Meyer, M. Liss, K.M. Kemner, *Chem. Geol.* 209 (2004) 107–119.
- [24] J.B. Fein, J.F. Boily, N. Yee, D. Gorman-Lewis, B. Turner, *Geochim. Cosmochim. Acta*, in press.
- [25] J.C. Westall, FITEQL, A Computer Program for Determination for Chemical Equilibrium Constants from Experimental Data, Version 2.0, Report 82-02, Department of Chemistry, Oregon State Univ., Corvallis, OR, 1982.
- [26] H.C. Helgeson, D.H. Kirkham, G.C. Flowers, *Am. J. Sci.* 281 (1981) 1249–1516.
- [27] C.F. Baes, R.E. Mesmer, *The Hydrolysis of Cations*, Wiley, New York, 1976.
- [28] T.J. Beveridge, R.G.E. Murray, *J. Bacteriol.* 141 (1980) 876–887.
- [29] T.J. Beveridge, W.S. Fyfe, *Can. J. Earth Sci.* 22 (1985) 1893–1898.
- [30] C. Hennig, P.J. Panak, T. Reich, A. Roberg, J. Raff, S. Selenska-Pobell, W. Matz, J.J. Bucher, G. Bernhard, H. Nitsche, *Radiochim. Acta* 89 (2001) 625–631.
- [31] M.I. Boyanov, S.D. Kelly, K. M Kemner, B.A. Bunker, J.B. Fein, D.A. Fowle, *Geochim. Cosmochim. Acta* 67 (2002) 3299–3311.
- [32] S.D. Kelly, K.M. Kemner, J.B. Fein, D.A. Fowle, M.I. Boyanov, B.A. Bunker, N. Yee, *Geochim. Cosmochim. Acta* 66 (2002) 3855–3871.
- [33] P.J. Panak, C.H. Booth, D.L. Caulder, J.J. Bucher, D.K. Shuh, H. Nitsche, *Radiochim. Acta* 90 (2002) 315–321.
- [34] W. Stumm, J.J. Morgan, *Aquatic Chemistry*, third ed., Wiley, New York, 1996.
- [35] J. Davis, R.O. James, J.O. Leckie, *J. Colloid Interface Sci.* 63 (1978) 480–499.
- [36] K.F. Hayes, G. Redden, W. Ela, J.O. Leckie, *J. Colloid Interface Sci.* 142 (1991) 448–469.
- [37] N. Sahai, D.A. Sverjensky, *Geochim. Cosmochim. Acta* 61 (1997) 2801–2826.
- [38] D. Borrok, J.B. Fein, C.F. Kulpa, *Environ. Sci. Technol.* 38 (2004) 5656–5664.
- [39] D.A. Dzombak, M.M. Morel, *Surface Complexation Modeling*, Wiley, New York, 1990.
- [40] C.J. Milne, D.G. Kinniburgh, E. Tipping, *Environ. Sci. Technol.* 35 (2001) 2049–2059.
- [41] D. Borrok, J.B. Fein, *Geochim. Cosmochim. Acta* 68 (2004) 3043–3053.
- [42] Z.S. Kooner, *Environ. Geol.* 21 (1993) 242–250.
- [43] J. Lützenkirchen, *J. Colloid Interface Sci.* 195 (1997) 149–155.
- [44] J.A. Dyer, P. Trivedi, N.C. Scrivner, D.L. Sparks, *Environ. Sci. Technol.* 37 (2003) 915–922.
- [45] R.D. Vanderweijden, C.H. Vanderweijden, R.N.J. Comans, *Mar. Chem.* 47 (1994) 65–79.
- [46] A.A. Rouff, R.J. Reeder, N.S. Fisher, *Aquat. Chem.* 8 (2002) 203–228.
- [47] R.W. Puls, R.M. Powell, D. Clark, C.J. Eldred, *Water Air Soil Pollut.* 57 (8) (1991) 423–430.
- [48] E. Spatharotis, C. Kallianou, *Comm. Soil Sci. Plant Anal.* 32 (2001) 3185–3205.
- [49] A.S. Mathuthu, J.H. Ephraim, *Talanta* 42 (1995) 1803–1810.
- [50] A. Liu, R.D. Gonzalez, *Langmuir* 16 (2000) 3902–3909.
- [51] J.A. Davis, J.A. Coston, D.B. Kent, C.C. Fuller, *Environ. Sci. Technol.* 32 (1998) 2820–2828.
- [52] J.A. Davis, D.E. Meece, M. Kohler, G.P. Curtis, *Geochim. Cosmochim. Acta* 68 (2004) 3621–3643.
- [53] J.C. Westall, J.D. Jones, G.D. Turner, J.M. Zachara, *Environ. Sci. Technol.* 24 (1995) 951–960.
- [54] D.B. Kent, R.H. Abrams, J.A. Davis, J.A. Coston, D.R. LeBlanc, *Water Resour. Res.* 36 (2000) 3411–3425.
- [55] B.A. Logue, R.W. Smith, J.C. Westall, *Appl. Geochem.*, in press.